International Journal of Biochemistry and Cell Biology 174 (2024) 106636

Contents lists available at ScienceDirect

International Journal of Biochemistry and Cell Biology

journal homepage: www.elsevier.com/locate/biocel

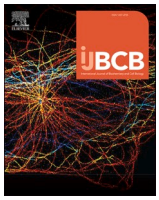

RNA-based logic for selective protein expression in senescent cells

Ward Jacobs [a], Masoomeh Khalifeh [a], Merijn Koot [a], Valentina Palacio-Castañeda [a,1], Jenny van Oostrum [a], Marleen Ansems [b], Wouter P.R. Verdurmen [a], Roland Brock [a,c,*]

[a] Department of Medical BioSciences, Radboud University Medical Center, Nijmegen 6525 GA, the Netherlands
[b] Radiotherapy and OncoImmunology Laboratory, Department of Radiation Oncology, Radboud University Medical Center, Nijmegen 6525 GA, the Netherlands
[c] Department of Medical Biochemistry, College of Medicine and Medical Sciences, Arabian Gulf University, Manama 329, Bahrain

ARTICLE INFO

Keywords:
Cellular senescence
Therapeutic mRNA
MiRNA
Nanomedicine

ABSTRACT

Cellular senescence is a cellular state characterized by irreversible growth arrest, resistance to apoptosis and secretion of inflammatory molecules, which is causally linked to the pathogenesis of many age-related diseases. Besides, there is accumulating evidence that selective removal of senescent cells can benefit therapies for cancer and fibrosis by modulating the inflammatory microenvironment. While the field of so-called senolytics has spawned promising small molecules and peptides for the selective removal of senescent cells, there is still no effective means to detect senescent cells *in vivo*, a prerequisite for understanding the role of senescence in pathophysiology and to assess the effectiveness of treatments aimed at removing senescent cells. Here, we present a strategy based on an mRNA logic circuit, that yields mRNA-dependent protein expression only when a senescence-specific miRNA signature is present. Following a validation of radiation-induced senescence induction in primary human fibroblasts, we identify miRNAs up- and downregulated in association with cellular senescence using RT-qPCR. Incorporating binding sites to these miRNAs into the 3' untranslated regions of the mRNA logic circuit, we demonstrate the senescence-specific expression of EGFP for detection of senescent cells and of a constitutively active caspase-3 for selective removal. Altogether, our results pave the way for a novel approach to execute an mRNA-based programme specifically in senescent cells aimed at their detection or selective removal.

1. Introduction

Cellular senescence is a functional state of non-proliferating cells with physiological but also high pathophysiological relevance (Childs et al., 2017). This state is associated with various sources of cellular damage, most notably DNA damage and among other functions, serves to prevent expansion of potentially malignant cells. DNA-damage signalling leads to p53- and Rb-dependent cell cycle arrest (Zhu et al., 2021). Key upregulated markers of senescence include cyclin-dependent kinase inhibitors $p16^{INK4A}$ and $p21^{WAF1/CIP1}$. Senescent cells often also display high β-galactosidase activity at pH 6.0, referred to as senescence-associated β-galactosidase (SA-β-gal) (Lee et al., 2006). Furthermore, senescent cells frequently secrete inflammatory factors such as IL-6 and IL-8 to communicate the compromized state to the surroundings, thereby promoting regeneration and immune clearance (Rodier et al., 2009). The totality of secreted factors is referred to as the senescence-associated secretory phenotype (SASP). Particularly in immunocompromized or aged individuals, the SASP may drive chronic inflammation in the tissue microenvironment (Rodier et al., 2009; Zhu et al., 2021).

Given the detrimental association with a number of pathologies including cancer, considerable research is being invested into the selective removal of senescent cells using so-called senolytics (Childs et al., 2017). Generally, senolytics interfere with survival-promoting pathways that are upregulated in senescent cells, thereby inducing apoptosis (Bousset and Gil, 2022). The first-generation approaches used existing small molecules including navitoclax, quercetin, dasatinib, fisetin and others (Kirkland and Tchkonia, 2020). Second-generation approaches were directed at small molecules that better distinguish senescent and non-senescent cells, leading to clinical trials in osteoarthritis and age-related macular degeneration (Zhang et al., 2022), however, with limited success. The latest generation of senolytics is more diverse and

* Correspondence to: Dept. of Medical BioSciences, Radboud University Medical Center, Geert Grooteplein 28, Nijmegen 6525 GA, the Netherlands.
E-mail address: roland.brock@radboudumc.nl (R. Brock).
[1] Present address: Oncode Institute, Jaarbeursplein 6, 3521 AL Utrecht, the Netherlands.

https://doi.org/10.1016/j.biocel.2024.106636
Received 17 January 2024; Received in revised form 21 June 2024; Accepted 29 July 2024
Available online 31 July 2024

includes peptide-based, antibody-based and gene-based therapies as well as approaches that train the immune system to recognize and remove senescent cells (Bousset and Gil, 2022; van Deursen, 2019). After an initial, rapid growth phase, progress has slowed due to an increasing realization of the complexity of cellular senescence *in vivo*, including variability between different types of senescent cells (van Deursen, 2019).

Very clearly, there is an urgent need for novel means to monitor senescent cells, in particular *in vivo*, and also for additional options to specifically eliminate senescent cells. It has been found that senescent cells possess specific miRNA signatures (Suh, 2018). miRNAs are useful indicators of phenotypic characteristics such as differentiation, inflammation, proliferation and epithelial-mesenchymal transition (Mahlab-Aviv et al., 2021; Faraonio et al., 2012; Zhang and Ma, 2012). miRNAs act in the posttranscriptional control of gene expression through binding to complementary sequences in the 3' untranslated repeats (UTRs) of the mRNAs, which leads to mRNA degradation. The same principle can also be employed for exogenously introduced *in vitro* transcribed mRNA (ivt mRNA). Here, sequences, complementary to cell state-specific miRNAs are incorporated into the 3' UTR of the ivt mRNA. Downregulation of an miRNA then leads to an increased stability of the mRNA and thus increased expression of the functional protein that the mRNA codes for. The dynamic range of this approach has been increased further by co-transfection of cells with an mRNA that encodes for a protein that further suppresses the expression of the functional protein (Matsuura et al., 2018; Wroblewska et al., 2015). One example for such mRNA-based regulatory circuits employs the protein L7Ae that binds to a stem-loop structure and thereby inhibits ribosome assembly (Saito et al., 2010).

Whereas interest in mRNA-based therapeutics is surging in vaccination and protein replacement as well as cell-based therapies (Beck et al., 2021; Chaudhary et al., 2021; Rohner et al., 2022; Vavilis et al., 2023; Wu et al., 2023), delivery strategies for mRNA still lack efficient cell-specific targeting for cells outside the liver (Loughrey and Dahlman, 2022; Paunovska et al., 2022; Żak and Zangi, 2021). For senescent cells, the challenge of reaching only these cells is aggravated by the fact that to this point, no sufficiently specific cell surface receptor has been identified. The incorporation of cell state-specific responsiveness into the delivered mRNA is a means to bypass the lack of selective delivery as irrespective of the cells that are reached, expression of a functional protein is restricted to those with the intended functional state.

In this project, we aimed to achieve selective expression of functional proteins in senescent cells. First, we confirmed the radiation-induced induction of cellular senescence in C5120 primary skin fibroblasts (Hernandez-Segura et al., 2017) and IMR-90 lung fibroblasts (Nichols et al., 1977). Then, we assessed senescence-induced changes in miRNA expression profiles. The binding site for an upregulated miRNA was incorporated into the 3'UTR of the L7Ae-encoding mRNA, the one for a downregulated miRNA into the 3'UTR of the functional protein-encoding mRNA. Senescence dependent expression was observed for both EGFP and a constitutively active caspase 3 as functional proteins, with the latter inducing senescence-specific cell death.

2. Materials and methods

2.1. Cell culture

Human C5120 primary skin fibroblasts were a gift from Dr. Rodenburg (Radboud University Medical Center, the Netherlands), IMR-90 primary lung fibroblasts were obtained from the American Type Culture Collection (ATCC). Cells were cultured in Medium 199 (Gibco, Waltham, MA, USA) supplemented with 10 % fetal calf serum (FCS, PAN-biotech, Aidenbach, Germany) and 1× penicillin/streptomycin (PenStrep, Merck, Burlington, MA, USA) (Distelmaier et al., 2012). Cells were cultured at 37 ℃ with 5 % CO_2.

2.2. Senescence induction by X-irradiation

Cells were collected by trypsinization, seeded at a density of 3000 cells/cm^2 and allowed to adhere overnight. The next day, cells were exposed to 6 or 18 gray (Gy) of ionizing radiation using an X-RAD 320ix Biological Irradiator (Precision X-Ray, Madison, CT, USA). Proliferating cells of identical passage number were used as controls. The induction of senescence was investigated 7 days after irradiation. Culture media was refreshed once at day 3 or 4 after irradiation.

2.3. Senescence-associated β-galactosidase staining

Seven days after irradiation, cells were fixed in a 12-well plate for 5 min at room temperature (RT) using 2 %/0.2 % formaldehyde/glutaraldehyde (w/w) in PBS, then washed twice with Hepes-buffered saline (HBS; 10 mM HEPES, 135 mM NaCl, 5 mM KCl, 5 mM $MgCl_2$, 1.8 mM $CaCl_2$). Staining solution (1 mg/mL 5-bromo-4-chloro-3-indolyl-β-D-galactopyranoside (X-gal), potassium ferrocyanide 5 mM, potassium ferricyanide 5 mM, NaCl 150 mM, $MgCl_2$ 2 mM, citric acid/sodium phosphate buffer, pH 6 40 mM) was prepared fresh, pre-heated to 37 ℃, and passed through a 0.45 μm filter to prevent crystallization. The plate was sealed with parafilm and aluminium foil and incubated for 16 h at 37 ℃, atmospheric CO_2. After 16 h, the cells were washed and assessed for blue staining using conventional light microscopy (see 2.9).

2.4. RNA extraction

Total RNA was extracted via guanidinium thiocyanate-phenol-chloroform extraction. Cells were lysed in a 25 cm^2 culture flask with TRI Reagent (Merck), after which the lysates where homogenized and incubated for 5 min at room temperature to allow dissociation of all nucleoprotein complexes. Phase separation was achieved by addition of chloroform and vigorous shaking, before incubation for 3 min at RT and centrifugation at 12,000×*g* and 4 ℃ for 15 min. RNA was precipitated from the aqueous phase using isopropanol by incubating 10 min at RT and centrifugation at 12,000×*g* and 4 ℃ for 25 min. The colourless precipitate was washed with EtOH/RNase-free water (75:25 v/v) at 7500×*g* and 4 ℃ for 5 min. The RNA was air-dried and resuspended in RNase-free water followed by a 10-min incubation at 55 ℃, then stored at −20 ℃. Total RNA concentration, purity, and quality were assessed using a Qubit 4.0 fluorometer (Invitrogen, Carlsbad, CA, USA), Nanodrop 2000 (Thermo Fisher Scientific, Waltham, MA, USA; Supplemental Table S1) and bleach agarose gel electrophoresis, respectively (Supplemental Figure S1).

2.5. Gene expression analysis

Total RNA (700 ng) was cleared of genomic DNA contamination by addition of DNase I reaction buffer (Invitrogen) and DNase I (Thermo Fisher Scientific) followed by 15 min incubation at RT. DNase treatment was halted by addition of ethylenediaminetetraacetic acid (EDTA; Invitrogen) and enzyme deactivation at 65 ℃ for 10 min. dNTPs (New England Biolabs, Ipswich, MA, USA) and random hexamer primers (Invitrogen) were added following denaturation for 5 min at 65 ℃ and cooling on ice to allow primer annealing. Reverse transcription was achieved by addition of RNase inhibitor (New England Biolabs), First Strand Buffer (Invitrogen), dithiothreitol (DTT, Invitrogen), and Superscript II Reverse Transcriptase (Invitrogen), then subjecting the 40 μL reaction volume to 10 min at 20 ℃, 59 min at 42 ℃, and 3 min at 95 ℃. RT-qPCR was performed in a CFX Connect Real-Time system (Bio-Rad, Hercules, CA, USA) by mixing primer pairs (425 nM each), IQ SYBR Green Supermix (Bio-Rad), Milli-Q, and 10× diluted cDNA (Supplemental Table 2). Relative expression levels were determined using the geometric mean of ACTB and HPRT1 as reference genes according to the Pfaffl equation (Pfaffl, 2001; Supplemental Figure S2).

2.6. miRNA profiling

100 ng of total RNA was mixed with miRNA-specific stem-loop primers (50 nM each, Supplemental Table 3); Sigma-Aldrich, Zwijndrecht, the Netherlands), RNase inhibitor, dNTPs, First Strand Buffer, Superscript II Reverse Transcriptase, and RNase-free water. Reverse transcription was achieved by subjecting the 7.5 μL reaction mixtures to 30 min at 16 ℃, 30 min at 42 ℃, and 5 min at 85 ℃. RT-qPCR was performed by mixing specific forward primers (300 nM), a universal reverse primer (300 nM), IQ SYBR Green Supermix, Milli-Q, and 17× diluted cDNA. Relative expression levels were determined using the geometric mean of miR-16–5p and miR-17–5p as reference miRNAs. These normalisation miRNAs were selected as the two most stable targets in the dataset using the GeNorm algorithm (Vandesompele et al., 2002; Supplemental Figure S3).

2.7. mRNA transfection

Transfections were performed in 8-well or 18-well μ-Slides (Ibidi, Gräfelfing, Germany). Lipofectamine MessengerMAX (LMM, Invitrogen) was mixed with OptiMEM (Gibco) and incubated at RT for 10 min. mRNA constructs were mixed with OptiMEM, then mixed with the LMM mixtures for 5 min at RT. The LMM-mRNA formulations were added to the cells in the appropriate, serum-containing and antibiotic-free media. Media were refreshed 2 h after particle addition. All custom mRNA constructs were purchased from RIBOPRO (Oss, Netherlands).

2.8. Fluorescence microscopy

16 h after transfection, cells were stained using Hoechst 33342 only (for EGFP experiments), or also with propidium iodide and calcein AM green (for rCasp3 experiments). Culture media was switched to OptiMEM, and microscopy was performed using a Leica SP8 SMD confocal microscope, with a 405 nm diode laser and white light laser at appropriate wavelengths for each dye and/or EGFP where applicable using HC PL Fluotar 10 x NA 0.3, 20 x NA 0.5 lenses.

2.9. Image processing and analysis

All images were processed and analysed using ImageJ software. The fraction of SA-β-gal, EGFP positive or dead cells was determined as described in supplemental methods.

2.10. Statistical analysis

Data processing was performed in Microsoft Excel, and statistical tests were performed using Graphpad Prism (GraphPad Software, version 7.0, San Diego, CA, USA). Since our experimental designs were comprized of matched pairs (irradiated vs. not irradiated), we assumed dependency for statistical testing. For all experiments, repeated measures one-way ANOVA was performed whenever a comparison was made between three irradiation groups, or between constructs in the transfection experiments. The ANOVA was followed by Dunnett's multiple comparison test to compare irradiated samples to their specific unirradiated counterpart, or Tukey's multiple comparison test when constructs were being compared against each other. For comparisons between two irradiation groups, paired two-tailed t-tests were performed. P-values were considered statistically significant when $\alpha < 0.05$. Statistical analyses for qPCR were always performed on the normalized data (normalisation strategies are explained above) and not on fold changes, as the results distribute normally in this format.

3. Results

3.1. Senescence markers emerge following exposure to X-irradiation

We selected two primary human fibroblast cell lines for establishing the concept of senescence-induced changes of miRNA-controlled mRNA expression. Fibroblasts are an important component of tumor stroma and cancer treatment such as irradiation can induce senescence in cancer-associated fibroblasts which may further promote tumor growth (Krtolica et al., 2001; Ruhland et al., 2016). Before devising our mRNA computational logic, we verified that ionizing radiation (IR) can robustly induce cellular senescence. First, we examined whether SA-β-gal activity was detectable in C5120 cells and IMR-90 lung fibroblasts seven days after 6 Gy or 18 Gy doses of IR. In both cell lines SA-β-gal activity increased for both 6 Gy and 18 Gy (Fig. 1).

Qualitatively, cells increased in size, and were flattened as shown by the lack of spindle 3D architectures usually present in proliferating fibroblast cultures; such morphological changes are commonly associated with cellular senescence (Noren Hooten and Evans, 2017).

Since SA-β-gal activity by itself is not sufficient to unequivocally confirm senescence induction, we additionally analyzed mRNA expression of senescence-associated cell cycle regulators *p16* and *p21*, and of two common SASP markers *IL-6* and *IL-8*. Through RT-qPCR, in both cell lines we found increased *p21* expression after 6 Gy and 18 Gy. *IL-8* levels were increased in C5120 cells upon 6 Gy (6.1-fold, $p=0.027$) and 18 Gy (5.6-fold, $p=0.010$; Fig. 2A). By comparison, in IMR-90 cells only *IL-6* expression was increased slightly upon 18 Gy irradiation demonstrating differences between these cell lines in their response to irradiation (Fig. 2C). Expression of *p16* was only slightly increased. By further examining the normalized raw data, we noticed that upregulated markers were not only expressed more on average, but also increased for each individual irradiation experiment in most cases (Fig. 2B, D).

3.2. miRNA profiles change by the cellular senescence programme

After validating senescence induction by IR, we applied this approach to detect senescence-regulated miRNAs that we could exploit for the mRNA computational logic. From literature, we identified a focused panel of candidate miRNAs (Faraonio et al., 2012; Greussing et al., 2013; Marasa et al., 2009; Olivieri et al., 2013; Wang et al., 2011) and determined their relative expression levels after exposure to 18 Gy IR using stem-loop RT-qPCR (Chen et al., 2005). Emphasis was placed on experiments using 18 Gy, as it demonstrated a more prominent senescence phenotype compared to 6 Gy, without apparent signs of toxicity. For the design of our circuit we aimed for a miRNA with a large fold-change and a low p-value (Fig. 3). In C5120 cells, the expression of miR-15b-5p and also miR-155–5p decreased upon exposure to 18 Gy. In IMR-90 cells, 155–5p and 20a-5p were downregulated, however, downregulation was less pronounced than the one observed in C5120 cells. By comparison, IMR-90 cells showed a more prominent upregulation of miRNAs with 486–5p and 30e-5p demonstrating the strongest changes. Nevertheless, both miRNAs also showed upregulation in C5120 cells. For our regulatory circuit we selected miR-15b-5p and miR-30e-5p. We favored miR-15b-5p over miR-155–5p because of its higher down-regulation and miR-30e-5p over miR-486–5p due to its higher expression level, potentially having a stronger impact on an exogenously introduced mRNA.

3.3. Functional mRNA design

Based on the information obtained for the changes in miRNA profiles, we designed mRNA constructs to establish proof-of-concept for our mRNA computational logic (Fig. 4). We aimed to first explore a detection tool, by constructing a logic circuit that acts as a senescence-responsive on-switch for EGFP expression. We rationalized that to assess the dynamics of selective EGFP expression in senescent cells,

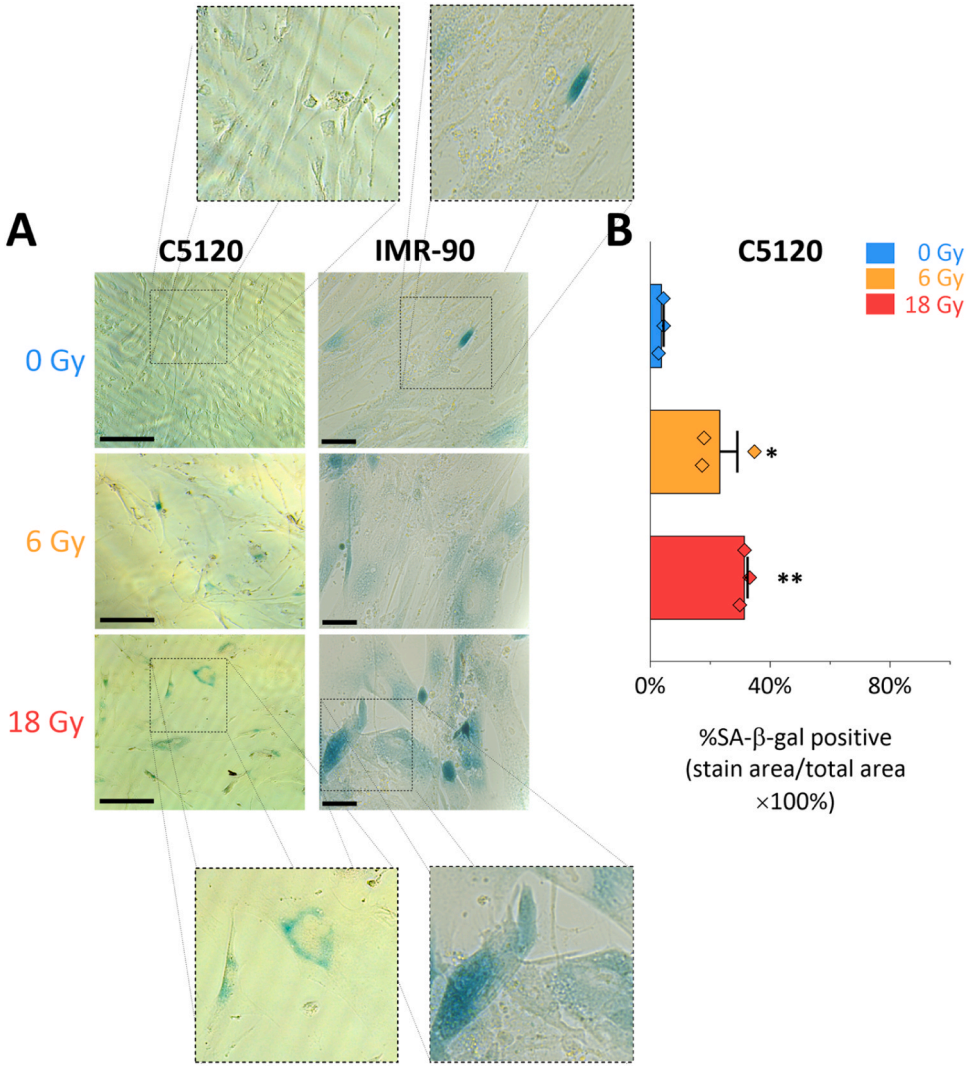

Fig. 1. Increased SA-β-gal activity following ionizing irradiation (IR). **(A)** Brightfield microscopy images following SA-β-gal staining of C5120 cells and IMR-90 lung fibroblasts exposed to the indicated doses of IR. Also note the morphological changes associated with senescence (see enlargements). Scale bars: 200 μm. **(B)** Quantification of stained area relative to total cellular area in C5120 cells. Each data point represents one of three individual irradiation experiments with 10 images per dose. Bars represent the mean, error bars the SEM, and significance levels represent p-values derived from t-tests (*p<0.05, **p<0.01). The ratio of positive cells increased 6.0-fold, p=0.024, for 6 Gy and 8.1-fold, p=0.007 for 18 Gy relative to the 0 Gy control.

rapid turnover would be desirable. For this reason, we used a destabilized EGFP by genetically fusing a PEST sequence from mouse ornithine decarboxylase ($MODC_{422–461}$) to its C-terminus (Li et al., 1998). As a non-responsive control, we designed an mRNA encoding only this EGFP-PEST (construct **1**, Table 1). Next, we designed construct **2**, which encodes the protein L7Ae from *A. fulgidus* (Huang and Lilley, 2013), connected to an mCherry-PEST via a T2A site. The T2A site is a self-cleaving peptide, which induces ribosome skipping to allow the expression of both proteins from a single open reading frame in a 1:1 ratio (Kim et al., 2011). Construct **2** was supplied with five response elements for miR-30e-5p, one in the 5'UTR, and four in the 3'UTR. All miRNA response elements are fully complementary to induce AGO2-mediated cleavage, which together with the specific positions in the mRNA sequence and a high miRNA load due to the multiple binding sites, has been shown to allow effective regulation of the mRNA (Matsuura et al., 2018; Meister et al., 2004). This design ensures that **2** will be efficiently degraded in senescent cells which upregulate miR-30e-5p. Construct **3** was an output mRNA encoding EGFP-PEST, but it also possessed two k-turn structural elements to which L7Ae can bind and repress its translation. Two k-turns allow stronger translational regulation than only one, especially when positioned close to the 5' end, and when combined with a Kozak sequence instead of other translational initiation sequences (Moore et al., 2004; Lilley, 2014; Saito et al., 2010). Lastly, **3** contained four fully complementary response elements for miR-15b-5p in its 3'UTR, so that this construct is degraded more slowly in senescent cells which downregulate miR-15b-5p. Altogether, constructs **2** and **3** would combine responsiveness to miR-30e-5p and miR-15b-5p, which both showed changes in expression in senescent cells of both cell lines, albeit to different extent, with the translation regulation of **3** by the L7Ae protein from **2**, to form a logic circuit for senescence-specific expression of the EGFP-PEST output (Fig. 4).

3.4. Selective labelling of senescent cells with a miRNA-responsive EGFP switch

Next, as a proof of concept for use in detection of senescent cells, we assessed the combination of constructs **2** and **3** as a logic circuit for senescence-selective EGFP expression in both cell lines. In a first step, we co-transfected cells with different ratios of **2** and **3** to identify the amount of **2** at which both efficient suppression in non-senescent cells and senescence-specific expression of **3** was achieved. Importantly, both mRNAs were co-formulated as it has been demonstrated that co-

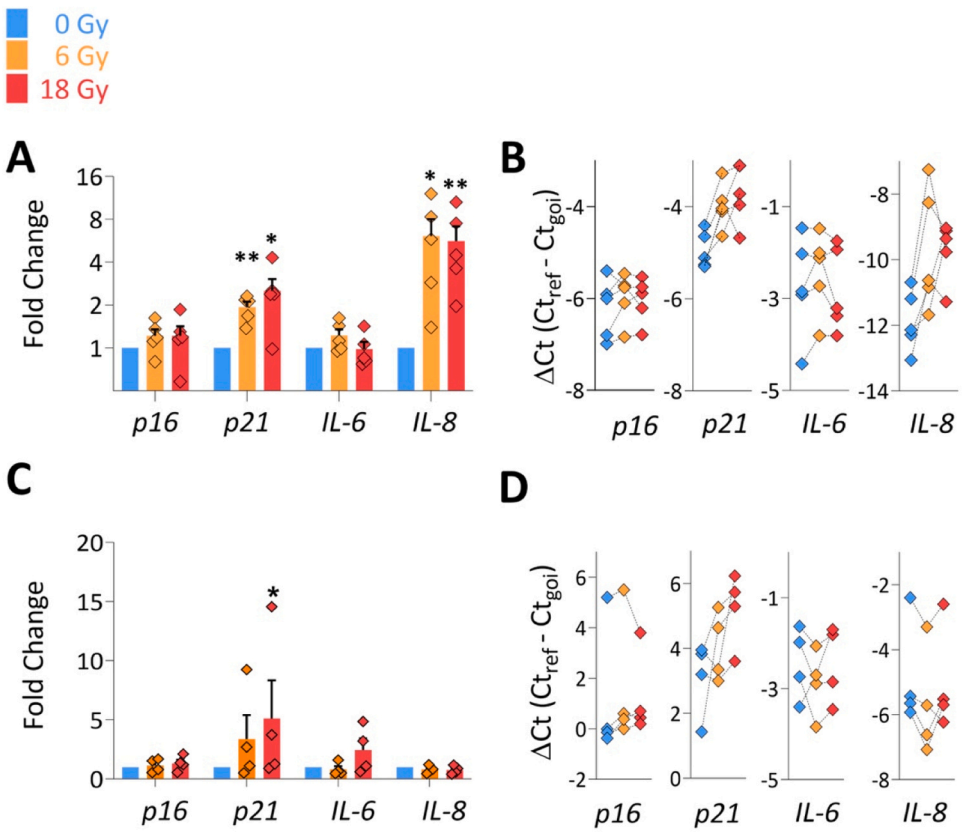

Fig. 2. Elevated mRNA levels of cell cycle and inflammatory markers associated with senescence after IR. **(A, C)** Fold changes for each gene of interest in (**A**) C5120 and (**C**) IMR-90 fibroblasts, normalized to the geometric mean of ACTB and HPRT1 (C5120) or HPRT1 (IMR-90). Data points represent five independent irradiation experiments, bars their mean, error bars the SEM (*p<0.05, **p<0.01). **(B, D)** Normalized raw measurements for (**B**) C5120 and (**D**) IMR-90 cells, where connected points were derived from the same irradiation experiment.

formulation is more reliable in delivering several mRNAs at intended ratios than treatment of cells with two separately formulated mRNAs (Zhang et al., 2022). As we went from a 1:1 ratio of **2**/**3**, towards 1:16 of **2**/**3**, the EGFP-PEST expression increased and ultimately resembled the condition for only **3** (Supplemental Figures S5, S6). This result demonstrated that the L7Ae protein encoded in **2** was indeed expressed and able to repress the EGFP-PEST expression from **3**. Detection of mCherry expression was challenging, likely attributed to too rapid turn-over due to the PEST sequence. At a ratio 1:4 of **2**/**3**, we observed the most senescence-specific EGFP-PEST expression.

To further support that the change in EGFP expression was senescence specific, we then co-transfected senescent C5120 cells with a combination of **2**+**3** or **1**+**2**. We also took along construct **3** alone, to evaluate whether selective EGFP expression is owed only to miR-15b-5p regulating construct **3**, or if miR-30e-5p regulating construct **2** also contributes, and construct **1** alone. Sixteen hours after transfection, we examined EGFP expression by fluorescence microscopy. Co-transfection with **2**+**3** led to strong expression after 18 Gy whereas in unirradiated cells it did not (Fig. 5A and Supplemental Figure S7). By comparison, co-transfection of **2**+**1**, did not result in a radiation-dependent increase of EGFP expression consistent with the absence of k-turns and miRNA response elements in **1**. These visual impressions were confirmed by digital image analysis. Co-transfection with **2**+**3** gave a 2-fold increase in EGFP expression after 18 Gy compared to 0 Gy (Fig. 5B) whereas for transfection with **3** alone, this difference was only 1.5-fold. This observation indicates that most of the selective EGFP expression was due to miR-15b-5p, which was also the miRNA with the strongest change in expression in senescent C5120 cells from our miRNA profiling, but miR-30e-5p further contributed to the increase. Since general expression levels differed largely between **3** and **1**, imaging of all transfections with **3** was performed with higher detector gain than of those with **1**. As such, a direct quantitative comparison between **1** and **3** cannot be made. Higher expression of construct **1** was likely due to the absence of miRNA binding sites and UTRs optimized for expression. For p21, we also confirmed the irradiation-induced increase determined by RT-qPCR by immunofluorescence in both fibroblast lines (Supplemental Figures S8, S9). Single-cell analysis for both EGFP and p21 demonstrated that the fraction of cells positive for both signals increases upon irradiation. However, there was no correlation of p21 and EGFP signal as one may potentially expect assuming that the most senescent cells also show the strongest response of the mRNA switch. We attribute this lack in correlation to heterogeneity in cell transfection that masks a potential correlation.

3.5. *Preferential elimination of senescent cells by a miRNA-responsive kill switch*

Lastly, we intended to demonstrate the senescence-selective elimination of cells. We conducted these experiments in the C5120 fibroblasts. To this end, we replaced EGFP-PEST in construct **3** with a constitutively active caspase-3 (rCasp3; construct **4**) or a protease dead mutant (construct **5**) (Srinivasula et al., 1998). Again, the first step was a titration of construct **2** relative to **4**, to confirm that L7Ae could suppress rCasp3, and to determine the ratio with the most selective induction of apoptosis. Sixteen hours after transfection, cells were stained with a live-dead dye combination (calcein AM green (live)/propidium iodide (dead)), and Hoechst (total). Using fluorescence microscopy, we observed an increase in propidium iodide-positive cells and a decrease in calcein AM-positive cells after 18 Gy when transfected with **2**+**4** (Fig. 6A, Supplemental Figure S10). Here, a 1:8 ratio for **2**/**4** led to the

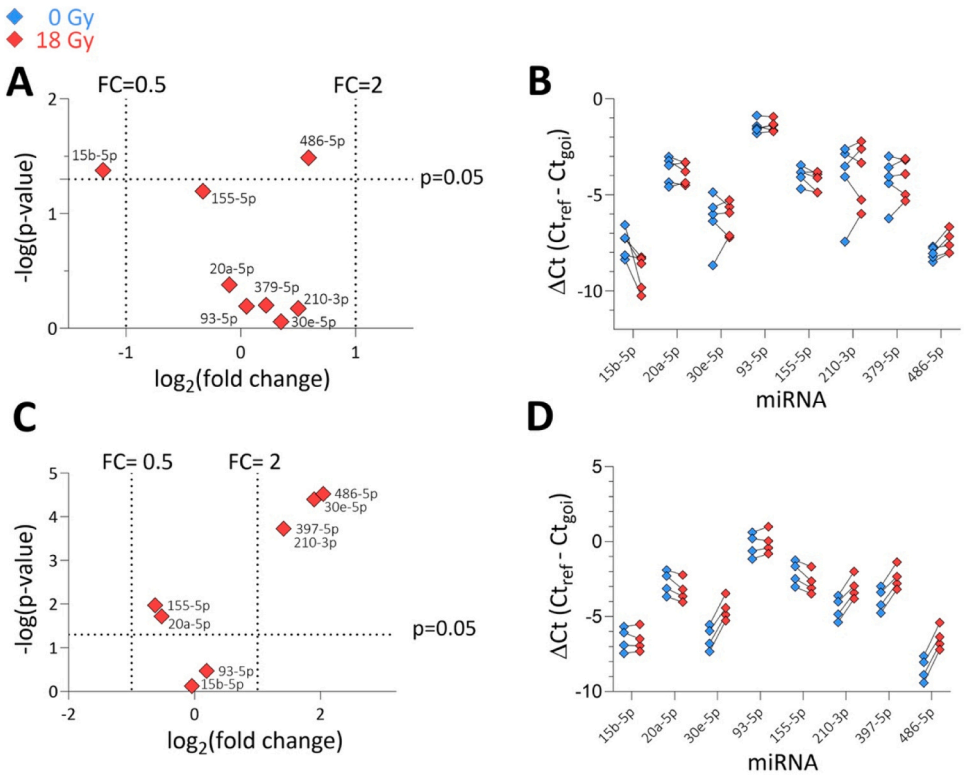

Fig. 3. Altered miRNA profiles in senescent cells. **(A, C)** Volcano plots showing the $\log_2$(fold change; FC) relative to 0 Gy on the x-axis, and -log(p-value) derived from t-tests on the y-axis for (**A**) C5120 and (**C**) IMR-90 cells. Ticks on the x and y axes represent the traditional cut-off values for targets ($0.5 \leq FC \vee FC \geq 2$, and $p < 0.05$); targets that comply with both criteria are therefore represented in the upper left and right quadrants. Each point represents the average from 5 independent irradiation experiments. (**B, D**) Normalized raw data of miRNA expression levels at 0 Gy (blue) and 18 Gy (red) for (**B**) C5120 and (**D**) IMR-90 cells, where connected points were derived from the same irradiation experiment to better illustrate the trends.

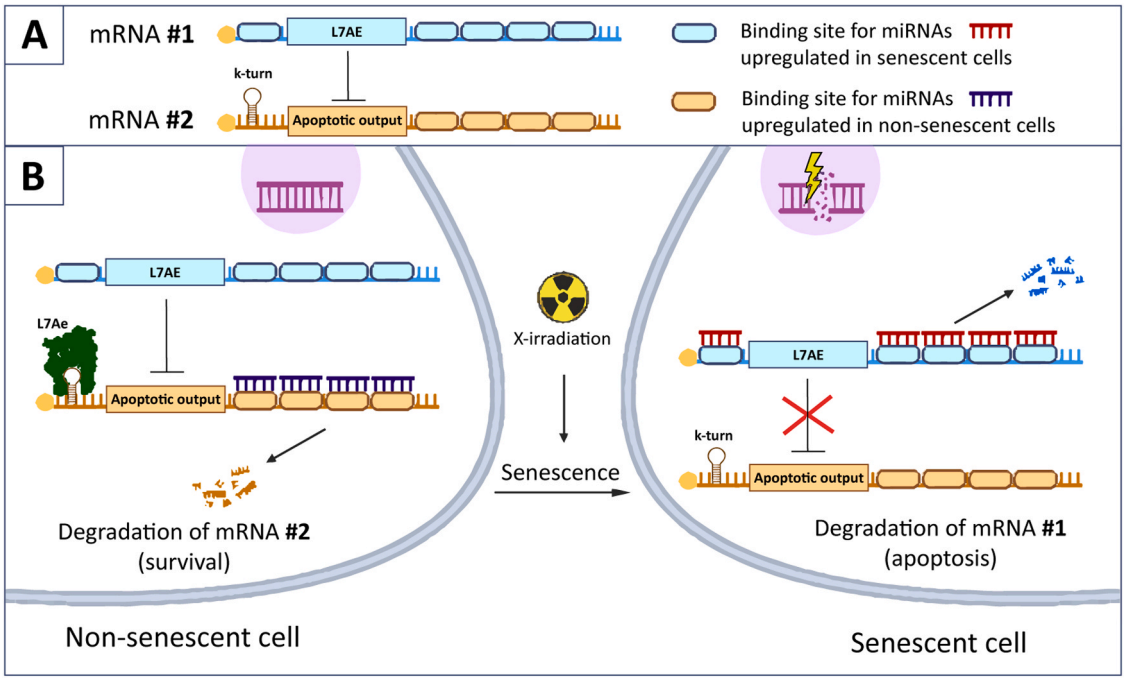

Fig. 4. Senescence-controlled mRNA expression. **(A)** Schematic of the mRNA design, where mRNA **#1** encodes L7Ae, which binds the k-turn in mRNA **#2** to repress its translation. While **#1** has response elements for miRNAs upregulated in senescent cells, **#2** contains binding sites for miRNAs upregulated in non-senescent cells. **(B)** When both mRNAs are delivered to senescent cells, **#1** is degraded and cannot repress **#2**, leading to apoptosis when mRNA #2 encodes an apoptosis inducer. In non-senescent cells, **#2** is degraded and repressed, allowing survival. The same principle, but with a detectable readout encoded via mRNA #2 (e.g., a fluorescent protein), can be employed to detect senescent cells.

Table 1
Overview of mRNA constructs designed and tested in this study. The left column shows the number for each construct, referred to in the main text. The middle column shows a schematic of the main functional elements in the construct; the full sequences can be found in Supplemental Figure S4. The right column lists the miRNA response elements in the constructs, to aid interpretation of our transfection experiments below.

Construct	Schematic	miRNA-dependence
1	EGFP-PEST	N/A
2	L7AE, mCherry-PEST	Binding site for miR-30e-5p TTTTT
3	2x k-turn, EGFP-PEST	Binding site for miR-15b-5p TTTTT
4	2x k-turn, rCasp3	Binding site for miR-15b-5p TTTTT
5	2x k-turn, rCasp3(mut)	Binding site for miR-15b-5p TTTTT

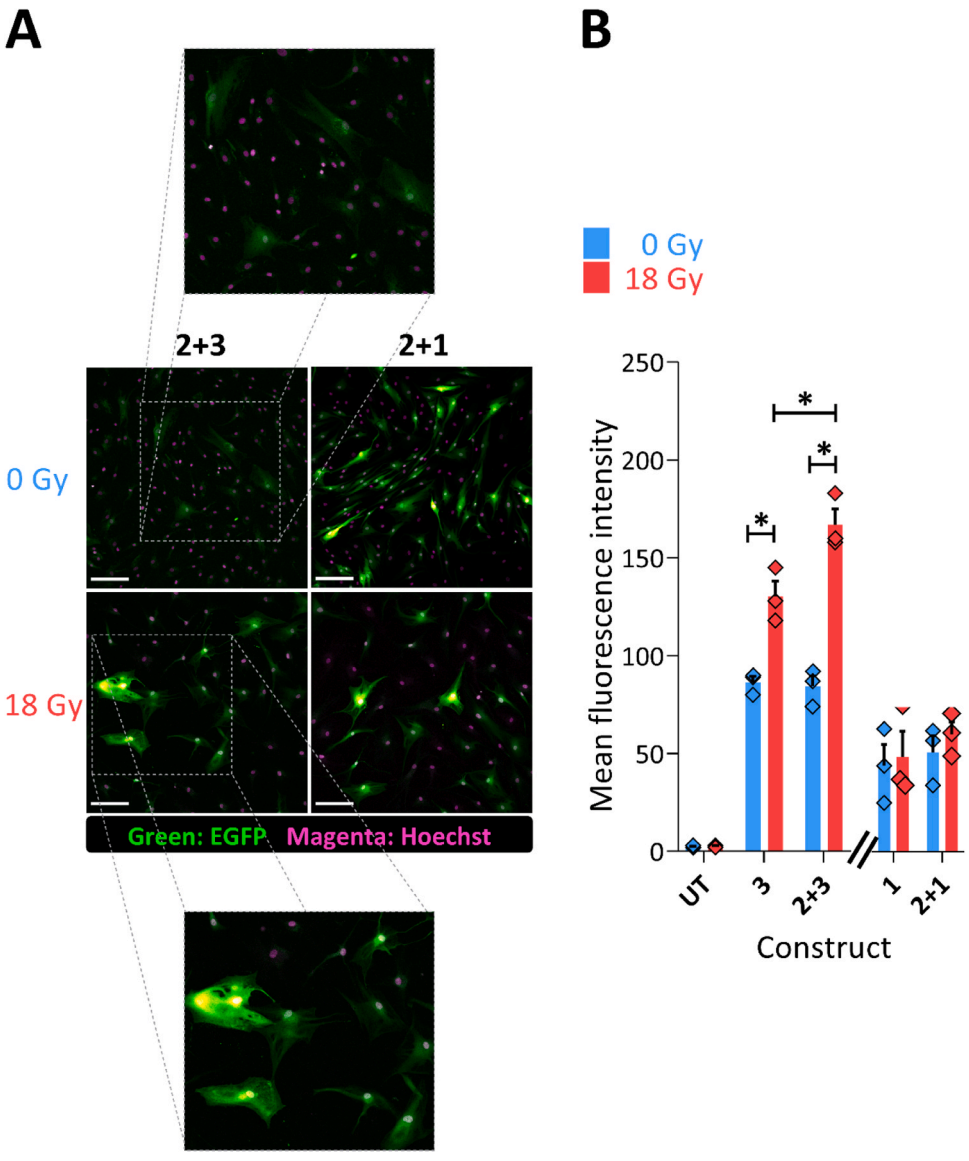

Fig. 5. Transfection of senescent cells with a miRNA-responsive EGFP switch. **(A)** Fluorescence microscopy to detect EGFP expression using a Hoechst counterstain for cell nuclei. Enlargements are shown to better visualize cell morphology. Scale bars: 200 μm. **(B)** Quantification of mean EGFP fluorescence intensity for each (combination of) construct(s). Mean intensities are calculated by total cellular area. Each point represents data from an independent irradiation experiment, bars their mean and error bars the SEM*$p<0.05$. See Fig. S7 for additional representative microscopy images.

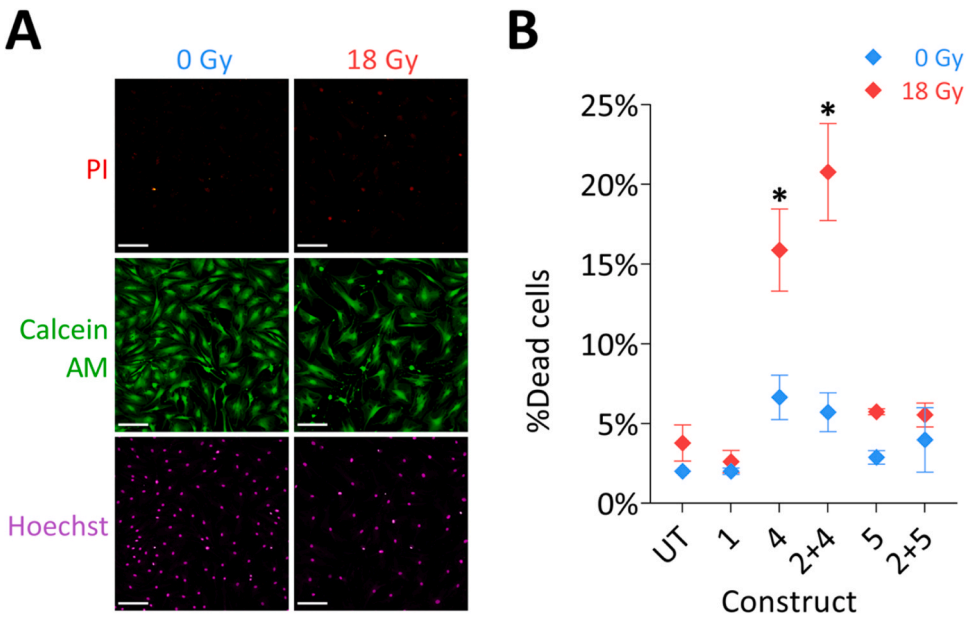

Fig. 6. Transfection of senescent cells with a miRNA-responsive kill switch. **(A)** Fluorescence microscopy images for C5120 stained with a live-dead dye combination (Calcein AM + PI) to detect apoptosis induction. Scale bars: 200 μm. **(B)** Quantification of dead (PI-positive) cells, relative to total cell number by Hoechst. Dots show the mean of three independent irradiation experiments and error bars the SEM. P-values are derived from t-tests or ANOVA where applicable (* $p<0.05$). See Fig. S7 for additional representative microscopy images of the conditions in **B**.

most selective senescence-dependent cell death (Supplemental Figure S11).

By co-transfecting senescent cells either with the **2**+**4** circuit, or with the circuit **2**+**5** or with constructs **4** and **5** alone, or with **1** as a non-apoptotic control mRNA, we demonstrated that **2**+**4** could indeed induce selective apoptosis in senescent cells (3.6-fold, p=0.022), whereas **2**+**5** could not. Construct **4** showed selectivity by itself owing to miR-15b-5p (2.4-fold, p=0.049), nevertheless, co-transfection with **2** increased senescence-specific cell death induction. Compellingly, the number of apoptotic cells in the 0 Gy group remained relatively close to the level of the untransfected condition, indicating the potential for our platform to avoid off-target effects.

4. Discussion

We here report the successful functional discrimination of senescent from non-senescent fibroblasts using a miRNA-responsive mRNA logic. Expression of EGFP as an example of a diagnostic marker and of constitutively active caspase-3 for removal of senescent cells as a potential therapeutic approach were achieved. Importantly, the same mRNA logic showed senescence responsiveness in two different fibroblast cell lines. These cell lines showed commonalities in the identity of differentially expressed miRNAs even though the extent of up- and downregulation differed for the individual miRNAs. While selective expression of output proteins in response to miRNA profiles by itself is not novel (Matsuura et al., 2018), we are to our knowledge the first to demonstrate such a strategy in regards to cellular senescence.

We validated induction of senescence via upregulation of SA-β-gal expression and expression of genes associated with senescence. There was a clear upregulation of *p21* in both fibroblast cell lines, whereas the increase of *p16* and *IL-6* expression was less pronounced and upregulation of *IL-8* expression was only observed in C5120 cells. These results may be explained by isolation of RNA 7 days after irradiation, as it has been described that some cell types require longer to express certain markers, and mechanistically *p21* upregulation is almost always detected before *p16* (Bourgeois and Madl, 2018). Moreover, detection of senescence markers can vary between the way of senescence induction (Hernandez-Segura et al., 2017). In particular senescence caused by DNA damage through irradiation involves a p21-dependent pathway (Chandra et al., 2022; Bai et al., 2020; Kumari and Jat, 2021; Ben-Porath and Weinberg, 2005). Further research will be required to understand to which degree the senescence-associated miRNA signature is stimulus and pathway dependent. In the course of our experiments we also noted that it makes a differences whether expression levels in senescent cells are referenced to non-irradiated cells for which mRNA is isolated 4 days after seeding or 7 days after seeding.

For IL-6, upregulation in primary fibroblasts is often detected (Childs et al., 2017; Hernandez-Segura et al., 2017). Absence of expression in our case may again be time-dependent since IL-6 is a late SASP marker (Childs et al., 2017).

Further research is required to identify the guiding principles for miRNA selection. The choice for miR-30e-5p was motivated from the observed upregulation and the relatively high expression level. The functional effect of the L7Ae mRNA confirms that our circuit responded to changes in miR-30e-5p levels. As a next step, we would like to better understand the interplay of fold-change and total expression level. Expression levels of miRNAs need to be sufficiently high to yield downregulation of target mRNAs. Thus one may want to favor a miRNA with a higher expression level but lower fold-change over a miRNA with a larger fold-change but lower expression level. Furthermore, the present selection of miRNAs was based on available literature data. Transcriptome-wide expression profiling may reveal cell and senescence stimulus-specific miRNAs undergoing larger changes in expression. Future experiments should also show to which degree the combination of the two different mRNAs increases the robustness towards variations in expression levels across cells.

Considering the only approximately 2-fold change in senescence-dependent EGFP levels, the level of selectivity of senescence-dependent induction of cell death was remarkable. For non-irradiated cells, the induction of cell death did not reach above background, providing a promising avenue for therapeutic applications. Possibly, senescent C5120 cells are more sensitive to the pro-apoptotic action of the executioner caspase, as downregulation of caspase 3 has been reported as a pro-survival mechanism of senescent cells (Marcotte et al., 2004). The implication for our approach would be a further enhancement of selectivity. Further experiments, also *in vivo* will be required to

define conditions that ensure maximum selectivity for senescent cells and avoidance of potential non-specific cell killing also due to leakage of effector protein expression.

Since our mRNAs can be adapted to the miRNA signature of any senescent cell type and can be designed to drive expression of any protein, our constructs provide a flexible and selective mRNA-based platform for use in therapies as a senolytic, or as diagnostic tool for *in vivo*-monitoring of senescent cells following therapy.

Accumulating evidence is showing that selective removal of senescent cancer-associated fibroblasts (CAFs) can alleviate multiple types of cancer (Hanley and Thomas, 2021; Meng et al., 2021). Most senolytics currently being evaluated are small molecules or peptides, normally targeting anti-apoptotic pathways such as variants related to the BH3 mimetic navitoclax (Wilson et al., 2010), or senescence maintenance effectors like the FOXO4-DRI (Baar et al., 2017). However, such agents cannot or only partly realize selectivity and cell type-specificity. Our platform could be applied to output proteins that target the same or other pathways much more specifically. This approach would combine the selectivity of the mRNA platform with the inherent selectivity of the output protein, to outclass smaller drugs in both efficacy and selectivity.

Further efforts will be needed to develop methods and protocols for the delivery of senescence-responsive mRNAs *in vivo*. Delivery through complexation with lipofectamine as employed here is restricted to *in vitro* applications. At present, the only clinically approved formulations for mRNA delivery are lipid nanoparticles as used in the siRNA drug Onpattro and the mRNA SARS-CoV-2 vaccines. Upon systemic injection, these LNPs show a strong propensity for the liver (Escalona-Rayo et al., 2024). For specific cell types, LNPs could be conjugated to targeting ligands (Kedmi et al., 2018). Furthermore, local application during surgery may be a viable option.

Aside from applications as a senolytic, a highly valuable implementation of our platform would be as a diagnostic tool. Detecting senescent cells is currently impossible *in vivo*. SA-β-gal staining requires biopsies and fixation *ex vivo* as does measuring mRNA or protein content from tissue sections (Gonzalez-Gualda et al., 2021). Some probes have been developed that can detect SA-β-gal *in vivo* in animal models like the fluorescent probe SPiDER-βgal (Doura et al., 2016) or the NIR-BG (Wang et al., 2019) probe. We could apply our platform to drive selective expression of a cell surface receptor, that can be detected with a corresponding systemic radiotracer ligand. This would allow senescence-specific labelling *in vivo,* with additional cell-type specificity in tissues accessible with mRNA, in a non-invasive fashion and independent of endogenous receptors or SA-β-gal. We therefore think that our approach can provide a valuable tool in diagnosing the senescent cell burden in age-related diseases, including cancer, as well as provide a much-needed non-invasive tool to investigate the true *in vivo* senolytic efficacy of the candidate senolytics agents that are currently being developed.

CRediT authorship contribution statement

Roland Brock: Writing – review & editing, Supervision, Resources, Project administration, Methodology, Funding acquisition, Conceptualization. **Masoomeh Khalifeh:** Investigation. **Ward Jacobs:** Writing – original draft, Validation, Methodology, Investigation, Formal analysis. **Merijn Koot:** Methodology, Investigation, Formal analysis. **Valentina Palacio-Castañeda:** Methodology. **Jenny van Oostrum:** Supervision, Methodology, Investigation. **Marleen Ansems:** Writing – review & editing, Resources, Methodology. **Wouter P. R. Verdurmen:** Writing – review & editing, Supervision, Methodology, Conceptualization.

Declaration of Competing Interest

The authors declare the following financial interests/personal relationships which may be considered as potential competing interests: Roland Brock reports financial support was provided by Dutch Science Foundation (OCENW.XS21.1.103) and the Dutch Cancer Society KWF (15274). Roland Brock reports a relationship with RiboPro B.V. that includes: board membership and equity or stocks. Roland Brock reports a relationship with Mercurna B. V. that includes: equity or stocks. If there are other authors, they declare that they have no known competing financial interests or personal relationships that could have appeared to influence the work reported in this paper.

Data availability

Data will be made available on request.

Acknowledgements

This project was supported by a grant from the Dutch Science Foundation (NWO-XS, OCENW.XS21.1.103) and from the Dutch Cancer Society KWF (15274).

Appendix A. Supporting information

Supplementary data associated with this article can be found in the online version at doi:10.1016/j.biocel.2024.106636.

References

Baar, M.P., Brandt, R.M.C., Putavet, D.A., Klein, J.D.D., Derks, K.W.J., Bourgeois, B.R.M., Stryeck, S., Rijksen, Y., van Willigenburg, H., Feijtel, D.A., van der Pluijm, I., Essers, J., van Cappellen, W.A., van, I.W.F., Houtsmuller, A.B., Pothof, J., de Bruin, R.W.F., Madl, T., Hoeijmakers, J.H.J., Campisi, J., de Keizer, P.L.J., 2017. Targeted apoptosis of senescent cells restores tissue homeostasis in response to chemotoxicity and aging. Cell 169 (1), 132–147.

Bai, J., Wang, Y., Wang, J., Zhai, J., He, F., Zhu, G., 2020. Irradiation-induced senescence of bone marrow mesenchymal stem cells aggravates osteogenic differentiation dysfunction via paracrine signaling. Am. J. Physiol. Cell Physiol. 318 (5), C1005–C1017.

Beck, J.D., Reidenbach, D., Salomon, N., Sahin, U., Tureci, O., Vormehr, M., Kranz, L.M., 2021. mRNA therapeutics in cancer immunotherapy. Mol. Cancer 20 (1), 69.

Ben-Porath, I., Weinberg, R.A., 2005. The signals and pathways activating cellular senescence. Int. J. Biochem. Cell Biol. 37 (5), 961–976.

Bourgeois, B., Madl, T., 2018. Regulation of cellular senescence via the FOXO4-p53 axis. FEBS Lett. 592 (12), 2083–2097.

Bousset, L., Gil, J., 2022. Targeting senescence as an anticancer therapy. Mol. Oncol.

Chandra, A., Lagnado, A.B., Farr, J.N., Doolittle, M., Tchkonia, T., Kirkland, J.L., LeBrasseur, N.K., Robbins, P.D., Niedernhofer, L.J., Ikeno, Y., Passos, J.F., Monroe, D.G., Pignolo, R.J., Khosla, S., 2022. Targeted clearance of p21- but not p16-positive senescent cells prevents radiation-induced osteoporosis and increased marrow adiposity. Aging Cell 21 (5), e13602.

Chaudhary, N., Weissman, D., Whitehead, K.A., 2021. mRNA vaccines for infectious diseases: principles, delivery and clinical translation. Nat. Rev. Drug Discov. 20 (11), 817–838.

Chen, C., Ridzon, D.A., Broomer, A.J., Zhou, Z., Lee, D.H., Nguyen, J.T., Barbisin, M., Xu, N.L., Mahuvakar, V.R., Andersen, M.R., Lao, K.Q., Livak, K.J., Guegler, K.J., 2005. Real-time quantification of microRNAs by stem-loop RT-PCR. Nucleic Acids Res. 33 (20), e179.

Childs, B.G., Gluscevic, M., Baker, D.J., Laberge, R.M., Marquess, D., Dananberg, J., van Deursen, J.M., 2017. Senescent cells: an emerging target for diseases of ageing. Nat. Rev. Drug Discov. 16 (10), 718–735.

Distelmaier, F., Valsecchi, F., Forkink, M., van Emst-de Vries, S., Swarts, H.G., Rodenburg, R.J., Verwiel, E.T., Smeitink, J.A., Willems, P.H., Koopman, W.J., 2012. Trolox-sensitive reactive oxygen species regulate mitochondrial morphology, oxidative phosphorylation and cytosolic calcium handling in healthy cells. Antioxid. Redox Signal 17 (12), 1657–1669.

Doura, T., Kamiya, M., Obata, F., Yamaguchi, Y., Hiyama, T.Y., Matsuda, T., Fukamizu, A., Noda, M., Miura, M., Urano, Y., 2016. Detection of LacZ-positive cells in living tissue with single-cell resolution. Angew. Chem. Int. Ed. Engl. 55 (33), 9620–9624.

Escalona-Rayo, O., Papadopoulou, P., Slutter, B., Kros, A., 2024. Biological recognition and cellular trafficking of targeted RNA-lipid nanoparticles. Curr. Opin. Biotechnol. 85, 103041.

Faraonio, R., Salerno, P., Passaro, F., Sedia, C., Iaccio, A., Bellelli, R., Nappi, T.C., Comegna, M., Romano, S., Salvatore, G., Santoro, M., Cimino, F., 2012. A set of miRNAs participates in the cellular senescence program in human diploid fibroblasts. Cell Death Differ. 19 (4), 713–721.

Gonzalez-Gualda, E., Baker, A.G., Fruk, L., Munoz-Espin, D., 2021. A guide to assessing cellular senescence in vitro and in vivo. FEBS J. 288 (1), 56–80.

Greussing, R., Hackl, M., Charoentong, P., Pauck, A., Monteforte, R., Cavinato, M., Hofer, E., Scheideler, M., Neuhaus, M., Micutkova, L., Mueck, C., Trajanoski, Z., Grillari, J., Jansen-Durr, P., 2013. Identification of microRNA-mRNA functional

interactions in UVB-induced senescence of human diploid fibroblasts. BMC Genom. 14, 224.
Hanley, C.J., Thomas, G.J., 2021. Targeting cancer associated fibroblasts to enhance immunotherapy: emerging strategies and future perspectives. Oncotarget 12 (14), 1427–1433.
Hernandez-Segura, A., de Jong, T.V., Melov, S., Guryev, V., Campisi, J., Demaria, M., 2017. Unmasking transcriptional heterogeneity in senescent cells. Curr. Biol. 27 (17), 2652–2660.
Huang, L., Lilley, D.M., 2013. The molecular recognition of kink-turn structure by the L7Ae class of proteins. RNA 19 (12), 1703–1710.
Kedmi, R., Veiga, N., Ramishetti, S., Goldsmith, M., Rosenblum, D., Dammes, N., Hazan-Halevy, I., Nahary, L., Leviatan-Ben-Arye, S., Harlev, M., Behlke, M., Benhar, I., Lieberman, J., Peer, D., 2018. A modular platform for targeted RNAi therapeutics. Nat. Nanotechnol. 13 (3), 214–219.
Kim, J.H., Lee, S.R., Li, L.H., Park, H.J., Park, J.H., Lee, K.Y., Kim, M.K., Shin, B.A., Choi, S.Y., 2011. High cleavage efficiency of a 2A peptide derived from porcine teschovirus-1 in human cell lines, zebrafish and mice. PLoS One 6 (4), e18556.
Kirkland, J.L., Tchkonia, T., 2020. Senolytic drugs: from discovery to translation. J. Intern. Med. 288 (5), 518–536.
Krtolica, A., Parrinello, S., Lockett, S., Desprez, P.Y., Campisi, J., 2001. Senescent fibroblasts promote epithelial cell growth and tumorigenesis: a link between cancer and aging. Proc. Natl. Acad. Sci. USA 98 (21), 12072–12077.
Kumari, R., Jat, P., 2021. Mechanisms of cellular senescence: cell cycle arrest and senescence associated secretory phenotype. Front. Cell Dev. Biol. 9, 645593.
Lee, B.Y., Han, J.A., Im, J.S., Morrone, A., Johung, K., Goodwin, E.C., Kleijer, W.J., DiMaio, D., Hwang, E.S., 2006. Senescence-associated beta-galactosidase is lysosomal beta-galactosidase. Aging Cell 5 (2), 187–195.
Li, X., Zhao, X., Fang, Y., Jiang, X., Duong, T., Fan, C., Huang, C.C., Kain, S.R., 1998. Generation of destabilized green fluorescent protein as a transcription reporter. J. Biol. Chem. 273 (52), 34970–34975.
Lilley, D.M., 2014. The K-turn motif in riboswitches and other RNA species. Biochim. Biophys. Acta 1839 (10), 995–1004.
Loughrey, D., Dahlman, J.E., 2022. Non-liver mRNA delivery. Acc. Chem. Res. 55 (1), 13–23.
Mahlab-Aviv, S., Linial, N., Linial, M., 2021. miRNA combinatorics and its role in cell state control-a probabilistic approach. Front. Mol. Biosci. 8, 772852.
Marasa, B.S., Srikantan, S., Masuda, K., Abdelmohsen, K., Kuwano, Y., Yang, X., Martindale, J.L., Rinker-Schaeffer, C.W., Gorospe, M., 2009. Increased MKK4 abundance with replicative senescence is linked to the joint reduction of multiple microRNAs. Sci. Signal 2 (94), ra69.
Marcotte, R., Lacelle, C., Wang, E., 2004. Senescent fibroblasts resist apoptosis by downregulating caspase-3. Mech. Ageing Dev. 125 (10-11), 777–783.
Matsuura, S., Ono, H., Kawasaki, S., Kuang, Y., Fujita, Y., Saito, H., 2018. Synthetic RNA-based logic computation in mammalian cells. Nat. Commun. 9 (1), 4847.
Meister, G., Landthaler, M., Patkaniowska, A., Dorsett, Y., Teng, G., Tuschl, T., 2004. Human Argonaute2 mediates RNA cleavage targeted by miRNAs and siRNAs. Mol. Cell 15 (2), 185–197.
Meng, J., Li, Y., Wan, C., Sun, Y., Dai, X., Huang, J., Hu, Y., Gao, Y., Wu, B., Zhang, Z., Jiang, K., Xu, S., Lovell, J.F., Hu, Y., Wu, G., Jin, H., Yang, K., 2021. Targeting senescence-like fibroblasts radiosensitizes non-small cell lung cancer and reduces radiation-induced pulmonary fibrosis. JCI Insight 6 (23).
Moore, T., Zhang, Y., Fenley, M.O., Li, H., 2004. Molecular basis of box C/D RNA-protein interactions; cocrystal structure of archaeal L7Ae and a box C/D RNA. Structure 12 (5), 807–818.
Nichols, W.W., Murphy, D.G., Cristofalo, V.J., Toji, L.H., Greene, A.E., Dwight, S.A., 1977. Characterization of a new human diploid cell strain, IMR-90. Science 196 (4285), 60–63.
Noren Hooten, N., Evans, M.K., 2017. Techniques to induce and quantify cellular senescence. J. Vis. Exp. 123.
Olivieri, F., Rippo, M.R., Monsurro, V., Salvioli, S., Capri, M., Procopio, A.D., Franceschi, C., 2013. MicroRNAs linking inflamm-aging, cellular senescence and cancer. Ageing Res. Rev. 12 (4), 1056–1068.
Paunovska, K., Loughrey, D., Dahlman, J.E., 2022. Drug delivery systems for RNA therapeutics. Nat. Rev. Genet 23 (5), 265–280.
Pfaffl, M.W., 2001. A new mathematical model for relative quantification in real-time RT-PCR. Nucleic Acids Res. 29 (9), e45.
Rodier, F., Coppe, J.P., Patil, C.K., Hoeijmakers, W.A., Munoz, D.P., Raza, S.R., Freund, A., Campeau, E., Davalos, A.R., Campisi, J., 2009. Persistent DNA damage signalling triggers senescence-associated inflammatory cytokine secretion. Nat. Cell Biol. 11 (8), 973–979.
Rohner, E., Yang, R., Foo, K.S., Goedel, A., Chien, K.R., 2022. Unlocking the promise of mRNA therapeutics. Nat. Biotechnol. 40 (11), 1586–1600.
Ruhland, M.K., Loza, A.J., Capietto, A.H., Luo, X., Knolhoff, B.L., Flanagan, K.C., Belt, B. A., Alspach, E., Leahy, K., Luo, J., Schaffer, A., Edwards, J.R., Longmore, G., Faccio, R., DeNardo, D.G., Stewart, S.A., 2016. Stromal senescence establishes an immunosuppressive microenvironment that drives tumorigenesis. Nat. Commun. 7, 11762.
Saito, H., Kobayashi, T., Hara, T., Fujita, Y., Hayashi, K., Furushima, R., Inoue, T., 2010. Synthetic translational regulation by an L7Ae-kink-turn RNP switch. Nat. Chem. Biol. 6 (1), 71–78.
Srinivasula, S.M., Ahmad, M., MacFarlane, M., Luo, Z., Huang, Z., Fernandes-Alnemri, T., Alnemri, E.S., 1998. Generation of constitutively active recombinant caspases-3 and -6 by rearrangement of their subunits. J. Biol. Chem. 273 (17), 10107–10111.
Suh, N., 2018. MicroRNA controls of cellular senescence. BMB Rep. 51 (10), 493–499.
Vandesompele, J., De Preter, K., Pattyn, F., Poppe, B., Van Roy, N., De Paepe, A., Speleman, F., 2002. Accurate normalization of real-time quantitative RT-PCR data by geometric averaging of multiple internal control genes. Genome Biol. 3 (7).
van Deursen, J.M., 2019. Senolytic therapies for healthy longevity. Science 364 (6441), 636–637.
Vavilis, T., Stamoula, E., Ainatzoglou, A., Sachinidis, A., Lamprinou, M., Dardalas, I., Vizirianakis, I.S., 2023. mRNA in the context of protein replacement therapy. Pharmaceutics 15 (1).
Wang, Y., Liu, J., Ma, X., Cui, C., Deenik, P.R., Henderson, P.K.P., Sigler, A.L., Cui, L., 2019. Real-time imaging of senescence in tumors with DNA damage. Sci. Rep. 9 (1), 2102.
Wang, Y., Scheiber, M.N., Neumann, C., Calin, G.A., Zhou, D., 2011. MicroRNA regulation of ionizing radiation-induced premature senescence. Int. J. Radiat. Oncol. Biol. Phys. 81 (3), 839–848.
Wilson, W.H., O'Connor, O.A., Czuczman, M.S., LaCasce, A.S., Gerecitano, J.F., Leonard, J.P., Tulpule, A., Dunleavy, K., Xiong, H., Chiu, Y.L., Cui, Y., Busman, T., Elmore, S.W., Rosenberg, S.H., Krivoshik, A.P., Enschede, S.H., Humerickhouse, R. A., 2010. Navitoclax, a targeted high-affinity inhibitor of BCL-2, in lymphoid malignancies: a phase 1 dose-escalation study of safety, pharmacokinetics, pharmacodynamics, and antitumour activity. Lancet Oncol. 11 (12), 1149–1159.
Wroblewska, L., Kitada, T., Endo, K., Siciliano, V., Stillo, B., Saito, H., Weiss, R., 2015. Mammalian synthetic circuits with RNA binding proteins for RNA-only delivery. Nat. Biotechnol. 33 (8), 839–841.
Wu, J., Wu, W., Zhou, B., Li, B., 2023. Chimeric antigen receptor therapy meets mRNA technology. Trends Biotechnol.
Żak, M.M., Zangi, L., 2021. Lipid Nanoparticles for Organ-Specific mRNA Therapeutic Delivery.
Zhang, H., Bussmann, J., Huhnke, F.H., Devoldere, J., Minnaert, A.K., Jiskoot, W., Serwane, F., Spatz, J., Roding, M., De Smedt, S.C., Braeckmans, K., Remaut, K., 2022. Together is better: mRNA Co-encapsulation in lipoplexes is required to obtain ratiometric co-delivery and protein expression on the single cell level. Adv. Sci. (Weinh.) 9 (4), e2102072.
Zhang, J., Ma, L., 2012. MicroRNA control of epithelial-mesenchymal transition and metastasis. Cancer Metastasis Rev. 31 (3-4), 653–662.
Zhang, L., Pitcher, L.E., Yousefzadeh, M.J., Niedernhofer, L.J., Robbins, P.D., Zhu, Y., 2022. Cellular senescence: a key therapeutic target in aging and diseases. J. Clin. Invest. 132 (15).
Zhu, X., Chen, Z., Shen, W., Huang, G., Sedivy, J.M., Wang, H., Ju, Z., 2021. Inflammation, epigenetics, and metabolism converge to cell senescence and ageing: the regulation and intervention. Signal Transduct. Target Ther. 6 (1), 245.